Available online at www.sciencedirect.com

SciVerse ScienceDirect

Ceramics International 39 (2013) 4163–4170

CERAMICS INTERNATIONAL

www.elsevier.com/locate/ceramint

Synthesis of spherical (30 nm) and rod-like (200 nm) zirconia co-reinforced mullite nanocomposites

Jie Zhong[a,b,c], Juan Zhao[b], Shuquan Liang[c,*], Xiaoping Tan[c], Manyuan Zhou[b], Guowei Zhang[c]

[a]*Wuhan National Laboratory for Optoelectronics, Huazhong University of Science and Technology, Wuhan 430074, PR China*
[b]*Department of Materials Engineering, Monash University, VIC 3800, Australia*
[c]*School of Materials Science and Engineering, Central South University, Changsha 410083, PR China*

Received 7 September 2012; received in revised form 22 October 2012; accepted 31 October 2012
Available online 24 November 2012

Abstract

The objective of this research is to study microstructure and phase evolution of zirconia–mullite (ZM) nanocomposites which were synthesized by the direct transformation from amorphous precursor monoliths. The monolithic precursors were heat treated at 950–1250 °C to obtain ZM composites. Scanning electron microscopy (SEM), energy-dispersive spectroscopy (EDS), transmission electron microscopy (TEM) and high resolution TEM (HRTEM) were employed to investigate the microstructure of the composites. A unique nano- and submicron-zirconia co-reinforced mullite composite microstructure was obtained after a controlled crystallization. The nano tetragonal zirconia (t-ZrO_2) grains (<50 nm) were spherical and embedded in the mullite lattice. The unconfined zirconia grains showed a preferred growth direction along $\langle 1\,0\,0 \rangle$ direction of t-ZrO_2, and formed submicron grains (<650 nm) with bar-like shape. The precursor derived ZM composites also demonstrated enhanced mechanical properties comparing with the conventional powder processed ZM composites.

Keywords: B. Nanocomposites; C. Mechanical properties; D. Zirconia; D. Mullite; Precursor transformation

1. Introduction

Over the past decades, mullite has been extensively investigated due to its outstanding engineering properties, such as high melting point, good chemical and thermal stability, excellent high-temperature strength, high creep resistance and high corrosion stability [1–6]. However, its low toughness and susceptibility to flaw have greatly restricted its industrial applications as advanced structural ceramic. In order to reduce its inherent brittleness by improving toughness, numerous researches have been carried out to synthesize mullite-based composites by introducing other ceramics components, such as zirconia, silicon carbide and alumina etc. [4,6–12]. Among these composites, mullite–zirconia composite has attracted the widest attention because of its excellent fracture toughness, high hardness and strength at room temperature.

Several toughening mechanisms related to martensitic transformation (from tetragonal (t-ZrO_2) to monoclinic (m-ZrO_2)) are the origins why zirconia is included into various ceramics matrices as a toughening agent [13,14]. Various oxides, such as CeO_2, Y_2O_3, MgO and CaO etc., were studied to preserve tetragonal zirconia to room temperature by forming zirconia solid solution to enhance the toughening efficiency of ZrO_2 [15–18]. Moreover, secondary oxides could also improve the strength of ceramics through depressing m-ZrO_2 formation *via* the refining of ZrO_2 grains [19,20]. Apart from doping additives, ceramic manufacturing routes also played a key role on the properties control of ZM composites [6,21–24]. For instance, regarding to the densification techniques, recently developed spark plasma and microwave sintering could provide high energy within seconds. Those rapid sintering process can achieve the purpose of inhibiting the abnormal

*Corresponding author. Tel.: +86 731 88836069.
E-mail address: lsq@mail.csu.edu.cn (S. Liang).

0272-8842/$ - see front matter © 2013 Published by Elsevier Ltd and Techna Group S.r.l.
http://dx.doi.org/10.1016/j.ceramint.2012.10.272

grain growth and enhancing the mechanical properties by promoting the reaction rate [25,26].

It is well accepted that the mechanical properties of a material largely depend on its microstructures. Optimized microstructures, such as fine grains, low porosity, low abnormality etc. are usually required for ceramics to obtain enhanced strength and toughness. Many studies have shown that introducing nano sized phases to form nanocomposite materials could be an effective way to significantly enhance the mechanical properties of ceramics [27,28]. This is due to the toughening mechanisms existing in the smaller scale of second phase particles. Conventional powder-processed ZM ceramics, restricted by composition homogeneity of starting powder, are very difficult to obtain nano-sized matrix grains and/or second phase particles (zirconia) [11,18,29,30]. The normally generated micro- and sub-micro grains are not the supreme microstructure for acquiring ceramics with excellent mechanical properties (e.g., high strength and good fracture toughness). In contrast, the homogenous pre-ceramic precursor derived composite ceramic could be easily produced with nano-crystalline microstructures by controlling certain parameters [31–34].

In this manuscript, we report a simple and feasible method to fabricate novel nano/sub-micro ZM composite ceramic through a direct transformation of bulk amorphous precursor. The precursors could be easily mechanically processed into required shapes and which can be maintained in the following heat treatments. The mechanical properties, phase development and microstructure evolution of the ZM composites crystallized at different conditions were investigated in this work. Furthermore, based on the observations, a crystallization mechanism was proposed to elucidate the generation of the unique microstructure.

2. Experimental procedure

2.1. Samples preparation

To fabricate ceramic precursor, the commercial available oxide powders were mixed first and homogenized by a planetary ball milling with zirconia balls at 100 rpm for 10 h. The batch powder was consisted of 51% of SiO_2, 30.5% Al_2O_3, 9.5% ZrO_2, 5.8% MgO and 2.7% CaO (molar fractions). CaO and MgO powders were added to decrease the melting temperature of mixture and as the partial stabilizer for ZrO_2 [19]. Then the mixed powder was dried in an oven at 80 °C and then fused in a corundum crucible in an electrical furnace (Si–Mo rod heater) at the temperature around 1700 °C. To generate amorphous pre-ceramic monoliths, the homogeneous flux was poured into a designed steel mold and quenched in liquid nitrogen. The as-made precursor was transparent and maintained in the shape of the mold. No cracks were formed after quenching. Afterward, the amorphous bulks were heated to 950 °C at a rate of 10 °C/min and kept for 2 h, and then heat treated at higher temperature (1100–1250 °C, 5 °C/min) for two more hours to finish crystallization. The samples were named as ZM-X, where ZM means zirconia–mullite ceramics, and X stands for the crystallization temperature. For example, the sample ZM-1150 is zirconia–mullite ceramic pre-treated at 950 °C and crystallized at 1150 °C.

2.2. Characterization

XRD profiles were collected by a X-ray diffraction using Japanese D/MAX 2500VB diffractionmeter equipped with Ni-filtered Cu-K_α radiation at a scan rate of 2°/min and a step size of 0.02°. The volume fractions of tetragonal zirconia (V_t) were calculated by the following Eqs (1)–(3) [35].

$$V_t = 1 - V_m \tag{1}$$

$$V_m = \frac{PX_m}{1+(P-1)X_m} \tag{2}$$

$$X_m = \frac{I_{m(\bar{1}\,1\,1)} + I_{m(1\,1\,1)}}{I_{m(\bar{1}\,1\,1)} + I_{m(1\,1\,1)} + I_{t(1\,0\,1)}} \tag{3}$$

V_m is the volume fraction of m-ZrO_2. X_m is the integrated intensity ratio and $P=1.340$. I_m and I_t are the peak intensities of m-ZrO_2 and t-ZrO_2, respectively.

Fracture toughness was determined for all the samples using a Vicker's hardness tester at a load of 9.8 N (Micro-Duromat 4000). The Eq. (4) was used to calculate the fracture toughness [36].

$$K_{IC} = 0.0319\frac{P}{al^{1/2}} \tag{4}$$

P is the indenter load (N). a is the indentation half-diagonal length (m) and l is the average length of the generated cracks (m).

Flexural strength was obtained using a three-point bending on 3 mm thickness, 4 mm width and 35 mm length, with a 30 mm span. The crosshead of the test is 0.5 mm per minutes (CSS-44100 tensile machine). The quenched glass precursors were mechanically processed into $3 \times 4 \times 35$ mm direct after quenching and then crystallized for the bending test. The secondary electron and back scattering electron (BSE) images were acquired using a Siri-on200 microscope. Platinum was coated on the samples before the observation. TEM images and the EDS patterns were taken utilizing a Tecnai G220 S-TWIN instrument operated at 200 kV. The HRTEM images were obtained using a JEOL 3010 microscopy operated at 300 kV. A Gatan 691 precision ion polishing system was employed to prepare TEM samples.

3. Results

3.1. Phases and mechanical properties

The quenched ceramic precursor was amorphous, suggested by its XRD curve in Fig. 1. The precursor bulks

maintained non-crystalline after heat treatment at 950 °C, while they became less transparent, indicating the occurrence of nucleation. t-ZrO_2 (JCPDS #50–1089) was first crystallized at 1100 °C. And trace amounts of mullite (JCPDS #15–0776) and alumina (JCPDS #50–0741) were also detected at this temperature. The higher heating temperature at 1150 °C promoted the crystallization of mullite, and its well resolved peaks could be observed in the XRD pattern of ZM-1150. However, the alumina phase disappeared, which may be because of the crystallization of mullite. Cristobalite (JCPDS #27–0605) was crystallized and showed an intense peak at around 22° in the XRD pattern. The sharpened t-ZrO_2 (1 0 1) peak of ZM-1150 suggested the increasing zirconia grain size comparing with ZM-1100. This also resulted in the phase transformation of some overgrown t-ZrO_2 and formation of m-ZrO_2 (JCPDS #37–1484). Cordierite (JCPDS #13–0294) was formed in both ZM-1200 and ZM-1250. It is clear that higher temperature promoted the crystallization of m-ZrO_2, mullite and cordierite. The decreasing cristobalite peak intensity of ZM-1250 compared to ZM-1200 is caused by increasing proportion of crystallized cordierite.

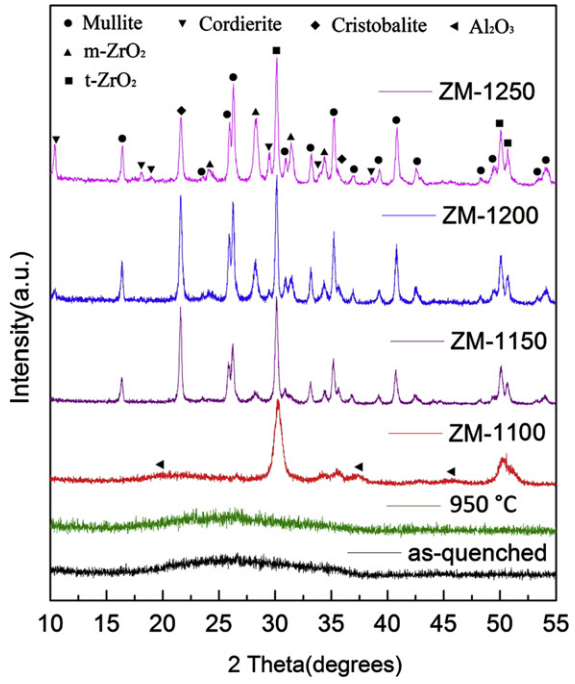

Fig. 1. X-ray diffraction patterns of samples treated at different conditions. The labeled samples were first treated at 950 °C before heat treated at denoted temperatures.

While this reduction of cristobalite intensity was not observed for ZM-1200 when the mullite crystallization fraction increased, indicating that the amorphous silica existed in ZM-1150 sample.

The mechanical properties and t-ZrO_2 volume proportions of different samples are shown in Table 1. The highest fracture toughness and flexural strength were obtained in ZM-1150 (5.13 ± 0.27 $MPam^{1/2}$ and 520 ± 35 MPa, respectively). The highest hardness, 1.35 ± 0.12 GPa, was achieved in ZM-1200. These obtained mechanical properties marked comparative improvement from the powder-sintered ZM composites, considering the low zirconia concentration in our samples [37]. With the increasing of heating temperature, the volume fractions of t-ZrO_2 decreased from 100% in ZM-1100 to 47% in ZM-1250.

3.2. Microstructure evolution

The microstructures of different samples were investigated by TEM observation. As can be noticed in Fig. 2a, a large quantity of nano crystals uniformly distributed in the ZM-1100 matrix. The inserted selected diffraction rings characterized that they were tetragonal zirconia, which was in consistence with the XRD result (Fig. 1). The average size of the t-ZrO_2 grains, shown in higher magnification image (Fig. 2b), is around 25 nm. It is very difficult to identify mullite and alumina in the TEM image due to their trace amounts.

Representative bright field TEM images of ZM-1150, ZM-1200 and ZM-1250 are shown in Fig. 3. The micromorphologies of ceramics changed dramatically when the crystallization temperature reached 1150 °C. Bar-like submicro grains (labeled as Z in the images) were randomly dispersed in these samples, and coarsened as the increasing of crystallization temperatures. Their darker color compared with other regions suggested their higher average atomic number (zirconium). Two more distinguishable phases were labeled in the TEM images. One was the bright phase with nano particles entrapped (M) and the other was grey phase bridging other phases (S).

In order to distinguish those phases, a series of EDS analysis were carried out for ZM-1150. The tests spots were denoted in Fig. 4a and the corresponding EDS curves were displayed in Fig. 4b. The detailed molar percentages of elements for the spots are recorded in Table 2. From spot-1 and spot-2 shown in Fig. 4b, the grey region was the silicon rich phase with aluminum, magnesium and calcium, indicating it was the parent phase of bulk precursor (S in Fig. 3).

Table 1
Mechanical properties and t-ZrO_2 volume percentages of samples heated at different temperature.

Samples	t-ZrO_2 (vol%)	ZrO_2 grain size (nm)	Hardness (GPa)	Fracture toughness ($MPam^{1/2}$)	Flexural strength (MPa)
ZM-1100	100	25	13.4 ± 1.4	4.92 ± 0.41	509 ± 17
ZM-1150	75	30, 200	12 ± 0.9	5.13 ± 0.27	520 ± 35
ZM-1200	61	30, 300	13.5 ± 1.2	4.65 ± 0.32	495 ± 23
ZM-1250	47	30, 450	10.1 ± 1.4	4.43 ± 0.54	487 ± 31

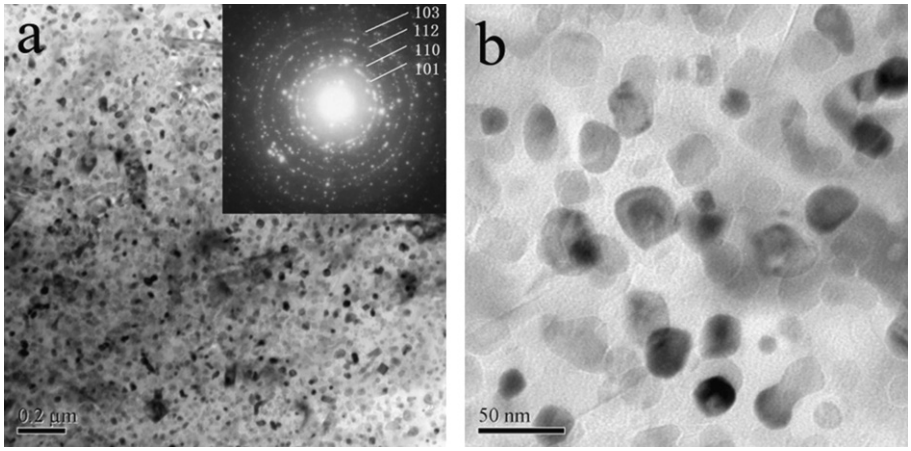

Fig. 2. TEM microstructures of ZM-1100 sample. (a) Low magnification morphology with selected area electron diffraction pattern inserted (t-ZrO_2), and (b) high magnification image showing homogenously dispersed nano t-ZrO_2 grains in the parent phase.

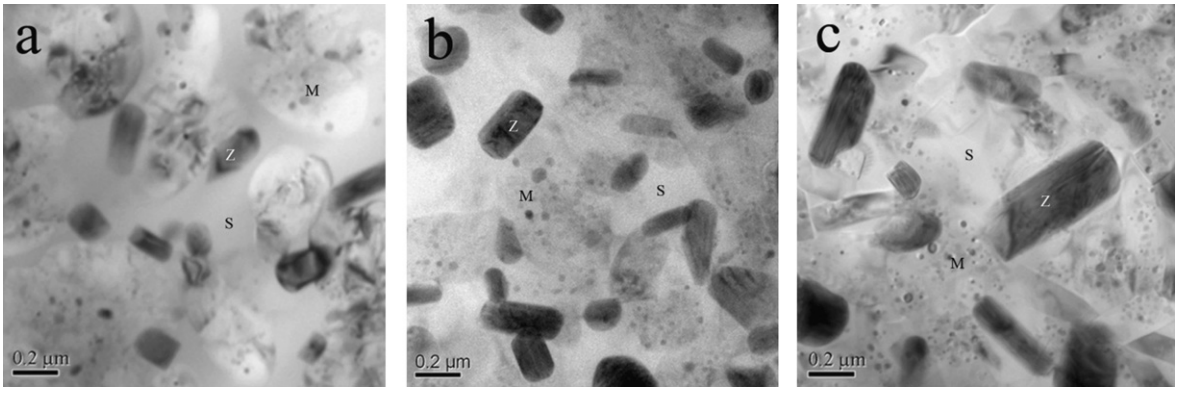

Fig. 3. TEM images of ZM-1150 (a), ZM-1200 (b) and ZM-1250 (c).

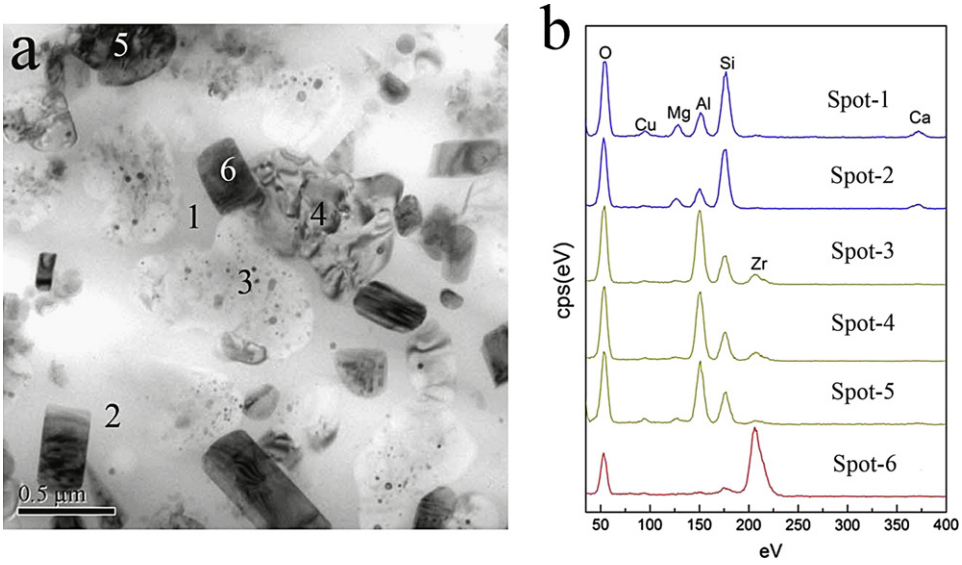

Fig. 4. TEM image of ZM-1150 with the labeled EDS spots (a) and their corresponding EDS curves (b).

In contrast, spots 3 to 5 displayed higher silicon and lower aluminum EDS intensities, which suggested they were alumina rich mullite (M in Fig. 3) [3]. It is interesting that there are very fine nano grains embedded in the mullite phases, similar to the reported TiN/ZTM materials [20]. The existence of zirconium peaks in their EDS patterns was the solid proof that the nano grains were zirconia (Fig. 4a). The morphology and size of those grains were

resembled to the t-ZrO_2 crystals in ZM-1100, which suggested they were nano sized t-ZrO_2. The bar-like dark crystals (Z in Fig. 3) were confirmed as zirconia as well by EDS test (spot-6). ZM-1150 still possessed high volume fractions of t-ZrO_2 up to 75%, which indicated only a small part of zirconia grains overgrew and transformed into m-ZrO_2. The area of the parent phase shown in Fig. 3b and c decreased and more zirconia and mullite crystals formed as the temperature increasing. The average zirconia grain sizes of samples were estimated from the TEM images and the results are shown in Table 1.

Fig. 5 shows the SEM and BSE morphologies of ZM-1200. The sample has been etched by 1% (volume fraction) hydrofluoric acid-water solution and washed with deionized water before observation. Silica and other non-crystalline phase have been removed after etching (Fig. 5a). The remained bright particles and grey irregular shaped regions were zirconia and mullite phases respectively. More distinctive morphologies of these two phases can be found in the corresponding BSE image in Fig. 5b. The finding in TEM that plenty of ultra-fine zirconia grains are confined in the mullite phase is confirmed by the BSE observation. The interior small white dots with arrows in Fig. 5b are t-ZrO_2 nano grains. The large zirconia grains can only be found at the mullite grains boundaries or in the matrix, which may suggest the formation of mullite restrict the grain growth of zirconia. This conjecture is supported by the observation that a few zirconia grains with the length up to 100 nm are trapped inside mullite grains during the coalescence of individual mullite crystals (Fig. 5a). On the other hand, the pinning effect of zirconia can also impede the grain growth of mullite phase.

Table 2
The detailed atomic percentages of elements for different EDS spots.

Elements	Spot 1	Spot 2	Spot 3	Spot 4	Spot 5	Spot 6
O	64.1	65.5	64.3	67.3	70.1	57.3
Mg	4.3	4.4	1.1	1.2	1.7	–
Al	7.1	6.7	18.4	18.1	16.0	–
Si	22	20.5	11.9	9.6	10.2	3.7
Ca	2.5	2.3	–	–	–	–
Zr	–	–	4.3	3.8	2.0	39.0

3.3. Growth of zirconia crystal

From the TEM images in Fig. 6, it is evident that the zirconia phase has different grain sizes and morphologies which are strongly related to where they are located. As shown in Fig. 6a, the intragranular zirconia are nano-sized

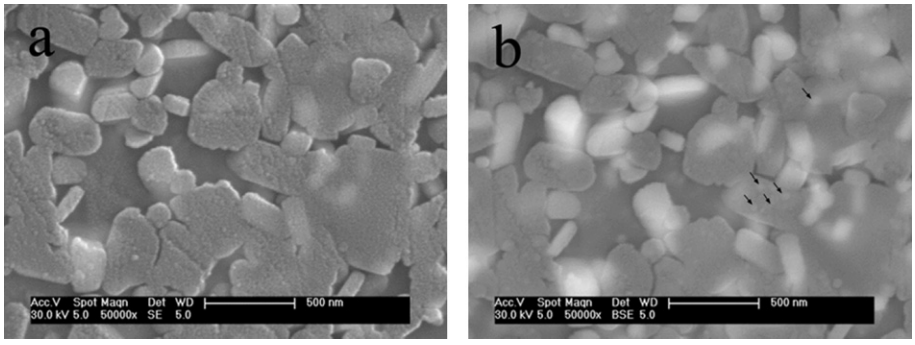

Fig. 5. SEM (a) and BSE (b) images of ZM-1200 showing the intergranular and intragranular zirconia grains.

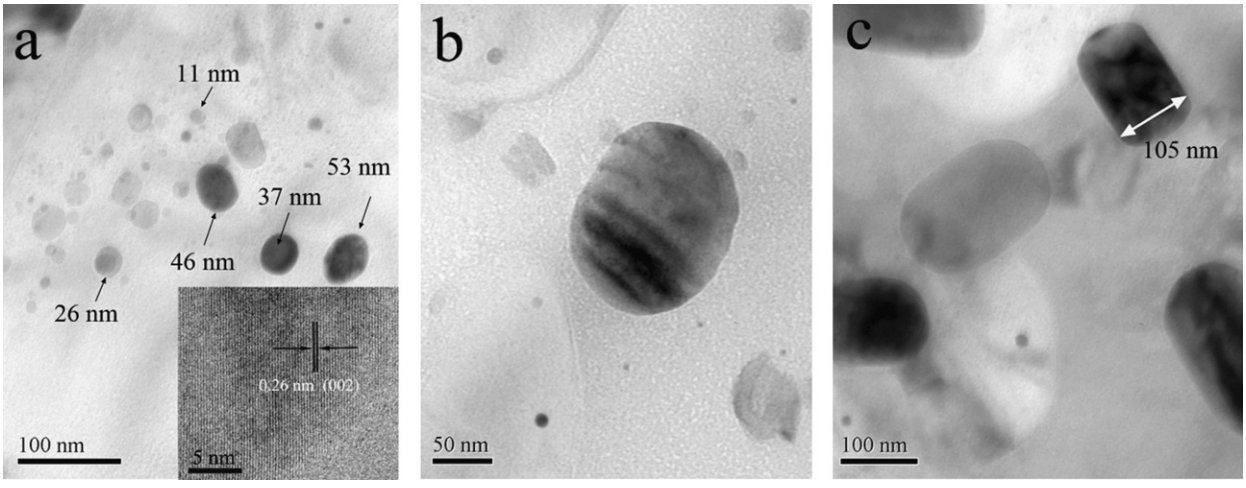

Fig. 6. Different TEM morphologies of zirconia grains. (a) Spherical, (b) elliptical-shaped and (c) short bar-like zirconia grains. Inset of (a) is the high magnification image of spherical zirconia.

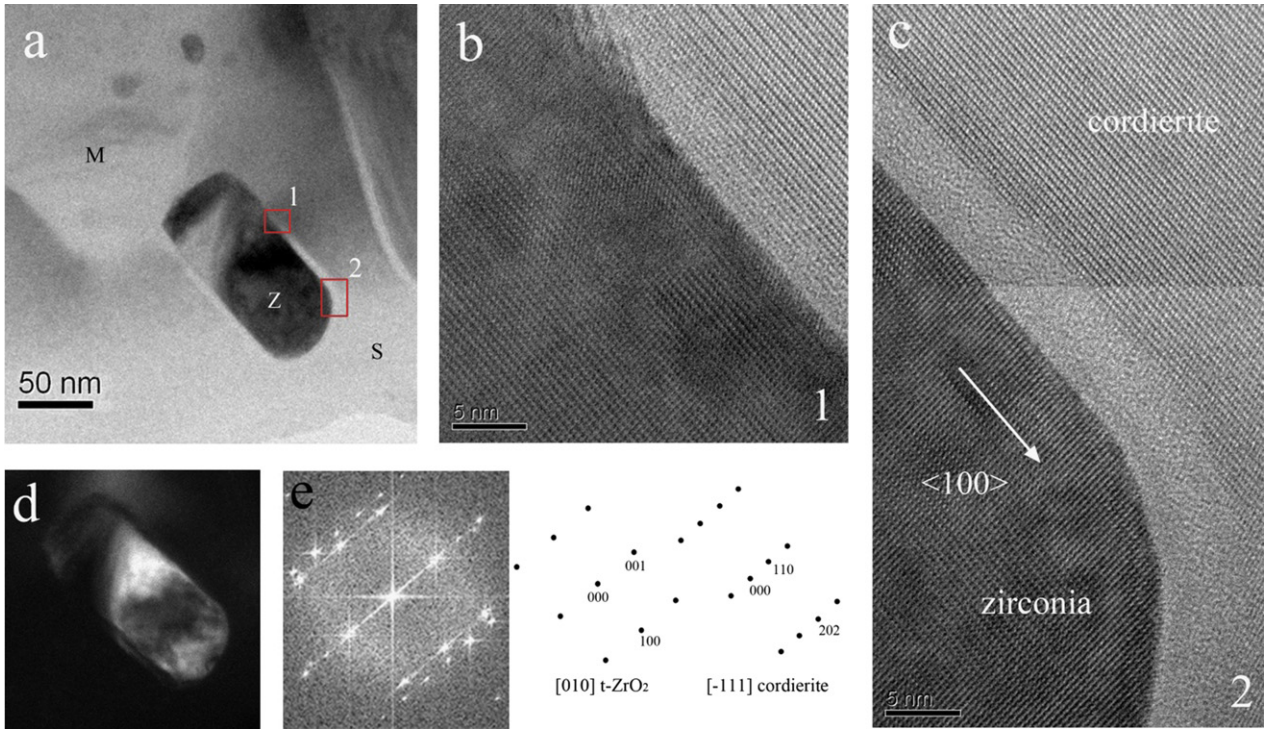

Fig. 7. (a) TEM morphology of ZM-1250. The denoted M, Z and S represent mullite, zirconia and parent phase, respectively. (b) High resolution TEM image of the grain boundary t-ZrO_2 with parent phase (cordierite) and (c) HRTEM image showing amorphous layer between those two phases. The corresponding areas of these HRTEM images in (a) are labeled as 1 and 2, respectively. (d) The dark field TEM image of t-ZrO_2 particle. (e) The corresponding fast Fourier transformed pattern of (b) and showing a parallel relation of t-ZrO_2 001 plane with cordierite 1 1 0 plane.

(< 50 nm) with spherical shape (see HRTEM image in Fig. S2). While the intergranular zirconia shows different morphology such as elliptical-shaped and bar-like grains (Fig. 6b, c). In general, the large zirconia grains have high aspect ratio, which indicates oriented growth of zirconia.

In order to understand the growth mechanism of zirconia grain, HRTEM images were obtained for a single zirconia crystal of ZM-1250, shown in Fig. 7b and c. Their corresponding areas were labeled in Fig. 7a. Fig. 7b shows the phase boundary structure of zirconia and matrix, which were identified as t-ZrO_2 and cordierite, respectively (Fig. 7e). The phase boundary between those two phases suggested that 0 0 1 plane of t-ZrO_2 was parallel with cordierite 1 1 0 plane (Fig. 7b). The rectilinear crystalline interface was gradually transformed into amorphous layer while the parallel relation was maintained. The thickness of amorphous layer surrounding the zirconia grain increased from less than 2 nm at the long edge to around 5 nm at the round top (Fig. 7c). This observation suggested the zirconia grew along $\langle 1\,0\,0 \rangle$ direction as labeled in the HRTEM image. This preferred growth direction attributes to the formation of bar-like particles from the spherical nano grains.

4. Discussion

Compared to the traditional powder sintering routes, the direct transformation from the amorphous bulks can achieve ultra-fine grains and unique nanostructures due to the high chemical homogeneity of starting precursor. Actually, the observations of two types of zirconia have been reported for power sintered ZM composites. In the reaction sintered ZM system, the size of intragranular zirconia grains reaches 300 nm, and these grains are embedded during the mullite grain growth, which is similar to the observation in our SEM morphology (Fig. 5) [36]. For the alkoxide-derived ZM composites, the decomposition of zircon is responsible for the formation intergranular zirconia [32]. A different microstructure formation mechanism should be applied for this amorphous precursor transformed ZM system.

The microstructure evolution from the amorphous precursor to ZM nanocomposites is proposed as follows. The liquid nitrogen quenched amorphous bulk has homogenous composition, as shown in Fig. 8a. However, this stressed metastable precursor tends to crystallize after nucleation. When heat treated at 1100 °C, nano size zirconia is first precipitated as the dispersoids from the parent phase (Fig. 8b). This diffusion controlled process results in composition gradient around zirconia grains. With further increase of heating temperature, mullite phase starts to crystallize around some nano zirconia due to its nuclei effect. Thus, the nano zirconia grains are confined in mullite grains. The solid state diffusion through mullite lattice becomes very difficult, which inhibits the growth of nano zirconia grains. Conversely, for those zirconia grains in parent phase, the diffusion is rapid, and consequently larger grains are produced. Due to assembly-like growth from the amorphous matrix, other than coalescence of

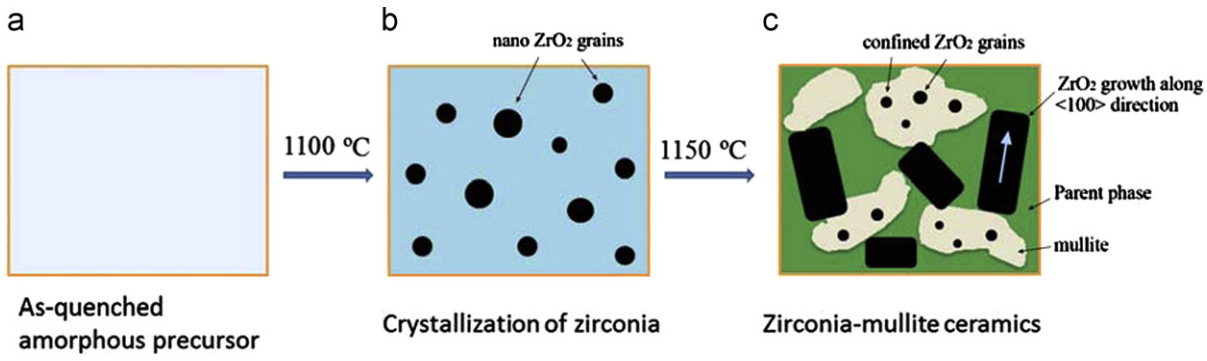

Fig. 8. Schematic crystallization process of amorphous precursor transformed zirconia–mullite ceramic. (a) Homogenous bulk precursor, (b) nano-crytalline zirconia dispersoids in the parent phase and (c) nano and sub-micro co-reinforced mullite composite. Please the note that the areas of color is not represented for the volume fractions of the phases.

individual grains in powder sintering process, the t-ZrO_2 preferentially grow along the direction of $\langle 1\,0\,0 \rangle$, which results in the formation of short bar shaped zirconia grain (Fig. 8c). This elongated grain morphology of zirconia is very different from the irregular shapes formed in sintered ZM ceramics [2,4,9,20]. The m-ZrO_2 is formed when the grain reaches the phase transformation size. The high heat treatment temperature promotes the growth of the zirconia, which reduces the volume fractions of t-ZrO_2 (Table 1).

High t-ZrO_2 fractions would enhance the mechanical properties of the composites due to phase transformation toughening mechanisms of zirconia [13]. Although ZM-1100 shows 100% t-ZrO_2, the best mechanical properties are obtained for the sample heat treated at 1150 °C (75% t-ZrO_2), when a nano and sub-micro zirconia ZM microstructures start to be developed. This indicates that both the bar-like t-ZrO_2 and the confined nano spherical zirconia grains provide reinforcement for the composite. Furthermore, the partially existed amorphous phase may also act as buffering agent for crystalline grains, which together functionalized as a multi-level "concrete" structure and result in well co-reinforced ZM composite ceramics.

5. Conclusion

High strength ZM nano-composite ceramics have been synthesized through the direct transformation of amorphous monolithic precursor. Benefited from the homogenous chemical composition of the precursor, sub-micro/nano-strucutred ZM ceramics were obtained through controlled crystallization. Two types of zirconia were generated in the composites. One was the spherical zirconia nano grains (~30 nm), which were confined in the mullite lattice. The other type zirconia grains oriented grew along the $\langle 1\,0\,0 \rangle$ (t-ZrO_2) direction, forming the bar shaped sub-micro particles (< 650 nm). This unique nanostructure contributed to high mechanical properties of sample ZM-1150, with fracture toughness and flexural strength up to 5.13 ± 0.27 MPam$^{1/2}$ and 520 ± 35 MPa, respectively. More importantly, this research demonstrated that the bulk precursor transformation was a feasible route to synthesize composite ceramics and achieve the purpose of refining the microstructures and improving the mechanical properties.

Acknowledgements

J. Z. acknowledges a scholarship from the China Scholarship Council and the financial support of national 863 plans of China.

References

[1] K.K. Chawla, Z.R. Xu, J.S. Ha, Processing, structure, and properties of mullite fiber mullite matrix composites, Journal of the European Ceramic Society 16 (2) (1996) 293–299.
[2] S.K. Zhao, Y. Huang, C.A. Wang, X.X. Huang, J.K. Guo, Mullite formation from reaction sintering of $ZrSiO_4$/alpha-Al_2O_3 mixtures, Materials Letters 57 (11) (2003) 1716–1722.
[3] H. Schneider, J. Schreuer, B. Hildmann, Structure and properties of mullite—a review, Journal of the European Ceramic Society 28 (2) (2008) 329–344.
[4] S. Bodhak, S. Bose, A. Bandyopadhyay, Densification study and mechanical properties of microwave-sintered mullite and mullite–zirconia composites, Journal of the American Ceramic Society 94 (1) (2011) 146–155.
[5] S. Li, H. Du, A. Guo, H. Xu, D. Yang, Preparation of self-reinforcement of porous mullite ceramics through in situ synthesis of mullite whisker in flyash body, Ceramics International 38 (2) (2012) 1027–1032.
[6] S. Prusty, D.K. Mishra, B.K. Mohapatra, G. Mishra, S.K. Singh, Preparation of fused zirconia/mullite aggregates from sillimanite, zircon, and alumina mixtures via plasma, Journal of the American Ceramic Society 95 (2) (2012) 530–537.
[7] R.S. Guo, Z.F. He, Z.F. Yang, Q.M. Yuan, Y.R. Chen, Controlling the flaw size and mechanical properties of ZTM/SiCp composites, Journal of the European Ceramic Society 16 (12) (1996) 1345–1349.
[8] X.H. Jin, L. Gao, L.H. Gui, J.K. Guo, Microstructure and mechanical properties of SiC/zirconia-toughened mullite nanocomposites prepared from mixtures of mullite gel, 2Y-TZP, and SiC nanopowders, Journal of Materials Research 17 (5) (2002) 1024–1029.
[9] N.M. Rendtorff, L.B. Garrido, E.F. Aglietti, Zirconia toughening of mullite–zirconia–zircon composites obtained by direct sintering, Ceramics International 36 (2) (2010) 781–788.

[10] C. Zanelli, M. Dondi, M. Raimondo, G. Guarini, Phase composition of alumina–mullite–zirconia refractory materials, Journal of the European Ceramic Society 30 (1) (2010) 29–35.
[11] G.I.V. Carbajal, J.L.R. Galicia, J.C.R. Angeles, J.L. Cuevas, C.A.G. Chavarria, Microstructure and mechanical behavior of alumina–zirconia–mullite refractory materials, Ceramics International 38 (2) (2012) 1617–1625.
[12] S. Gustafsson, L.K.L. Falk, J.E. Pitchford, W.J. Clegg, E. Liden, E. Carlstrom, Development of microstructure during creep of polycrystalline mullite and a nanocomposite mullite/5 vol% SiC, Journal of the European Ceramic Society 29 (4) (2009) 539–550.
[13] R.H.J. Hannink, P.M. Kelly, B.C. Muddle, Transformation toughening in zirconia-containing ceramics, Journal of the American Ceramic Society 83 (3) (2000) 461–487.
[14] B. Basu, Toughening of yttria-stabilised tetragonal zirconia ceramics, International Materials Reviews 50 (4) (2005) 239–256.
[15] S.C. Farmer, L.H. Schoenlein, A.H. Heuer, Precipitiation of $Mg_2Zr_5O_{12}$ in MgO-partially-stabilized ZrO_2, Journal of the American Ceramic Society 66 (7) (1983) C107–C109.
[16] J.M. Wu, C.M. Lin, Effect of CeO_2 on reaction-sintered mullite–ZrO_2 ceramics, Journal of Materials Science 26 (17) (1991) 4631–4636.
[17] K. Das, B. Mukherjee, G. Banerjee, Effect of yttria on mechanical and microstructural properties of reaction sintered mullite–zirconia composites, Journal of the European Ceramic Society 18 (12) (1998) 1771–1777.
[18] M. Imose, A. Ohta, Y. Takano, M. Yoshinaka, K. Hirota, O. Yamaguchi, Low-temperature sintering of mullite/yttria-doped zirconia composites in the mullite-rich region, Journal of the American Ceramic Society 81 (4) (1998) 1050–1052.
[19] S. Maitra, S. Pal, S. Nath, A. Pandey, R. Lodha, Role of MgO and Cr_2O_3 additives on the properties of zirconia–mullite composites, Ceramics International 28 (7) (2002) 819–826.
[20] X.H. Jin, L. Gao, J.G. Li, S. Zheng, Influence of microstructure evolution on the electroconducting behavior of intragranular TiN/ZTM nanocomposites, Journal of the American Ceramic Society 87 (1) (2004) 162–165.
[21] I.M. Low, R. McPherson, Crystallization of gel-derived mullite–zirconia composites, Journal of Materials Science 24 (3) (1989) 951–958.
[22] T. Ebadzadeh, Reaction sintering of multicomponent mixtures for producing ceramics containing zirconia, Journal of the European Ceramic Society 20 (6) (2000) 725–729.
[23] Y.J. Lin, Y.C. Chen, Cyclic infiltration of porous zirconia preforms with a liquid solution of mullite precursor, Journal of the American Ceramic Society 84 (1) (2001) 71–78.
[24] K.A. Khor, L.G. Yu, Y. Li, Z.L. Dong, Z.A. Munir, Spark plasma reaction sintering of ZrO_2–mullite composites from plasma spheroidized zircon/alumina powders, Materials Science and Engineering A—Structural Materials Properties Microstructure and Processing 339 (1-2) (2003) 286–296.
[25] M. Hotta, T. Goto, Densification, phase transformation and hardness of mullite-cubic BN composites prepared by spark plasma sintering, Journal of the Ceramic Society of Japan 118 (1374) (2010) 157–160.
[26] S. Akpinar, I.M. Kusoglu, O. Ertugrul, K. Onel, In situ mullite foam fabrication using microwave energy, Journal of the European Ceramic Society 32 (4) (2012) 843–848.
[27] D. Sarkar, S. Adak, M.C. Chu, S.J. Cho, N.K. Mitra, Influence of ZrO_2 on the thermo-mechanical response of nano-ZTA, Ceramics International 33 (2) (2007) 255–261.
[28] J.F. Bartolome, C.F. Gutierrez-Gonzalez, R. Torrecillas, Mechanical properties of alumina–zirconia–Nb micro-nano-hybrid composites, Composites Science and Technology 68 (6) (2008) 1392–1398.
[29] F. Sahnoune, H. Belhouchet, N. Saheb, M. Heraiz, M. Chegaar, P. Goeuriot, Phase transformation and sintering behaviour of mullite and mullite–zirconia composite materials, Advances in Applied Ceramics 110 (3) (2011) 175–180.
[30] T. Koyama, S. Hayashi, A. Yasumori, K. Okada, M. Schmucker, H. Schneider, Microstructure and mechanical properties of mullite/zirconia composites prepared from alumina and zircon under various firing conditions, Journal of the European Ceramic Society 16 (2) (1996) 231–237.
[31] G.H. Beall, L.R. Pinckney, Nanophase glass-ceramics, Journal of the American Ceramic Society 82 (1) (1999) 5–16.
[32] P. Colomban, L. Mazerolles, Nanocomposites in mullite–ZrO_2 and mullite–TiO_2 systems synthsized through alkoxide hydrolysis gel routes—microstrucrure and fractorgraphy, Journal of Materials Science 26 (13) (1991) 3503–3510.
[33] C.-C. Lin, A. Zangvil, R. Ruh, Phase and microstructure evolution in alkoxide-derived mullite/MgO-partially-stabilized zirconia, Journal of the American Ceramic Society 78 (5) (1995) 1361–1371.
[34] G. Parcianello, E. Bernardo, P. Colombo, Mullite/zirconia nanocomposites from a preceramic polymer and nanosized fillers, Journal of the American Ceramic Society 94 (5) (2011) 1357–1362.
[35] H. Toraya, M. Yoshimura, S. Somiya, Calibration curve for quantitative analysis of the monoclinic-tertragonal ZrO_2 system by X-ray diffraction, Journal of the American Ceramic Society 6 (2) (1984) 112–119.
[36] C.B. Ponton, R.D. Rawlings, Vickers indentation fracture toughness test. Part 1. Review of literature and formulation of standardised indentation toughness equations, Materials Science and Technology 5 (9) (1989) 865–872.
[37] N.M. Rendtorff, L.B. Garrido, E.F. Aglietti, Mechanical and fracture properties of zircon–mullite composites obtained by direct sintering, Ceramics International 35 (7) (2009) 2907–2913.